HAL open science

Remote sensing of suspended particulate matter in turbid oyster-farming ecosystems

Pierre Gernez, Laurent Barillé, Astrid Lerouxel, Constant Mazeran, Axel Lucas, David Doxaran

To cite this version:

Pierre Gernez, Laurent Barillé, Astrid Lerouxel, Constant Mazeran, Axel Lucas, et al.. Remote sensing of suspended particulate matter in turbid oyster-farming ecosystems. Journal of Geophysical Research. Oceans, 2014, 119 (10), pp.7277-7294. 10.1002/2014JC010055 . hal-03502761

HAL Id: hal-03502761

https://hal.science/hal-03502761

Submitted on 26 Dec 2021

HAL is a multi-disciplinary open access archive for the deposit and dissemination of scientific research documents, whether they are published or not. The documents may come from teaching and research institutions in France or abroad, or from public or private research centers.

L'archive ouverte pluridisciplinaire **HAL**, est destinée au dépôt et à la diffusion de documents scientifiques de niveau recherche, publiés ou non, émanant des établissements d'enseignement et de recherche français ou étrangers, des laboratoires publics ou privés.

Copyright

AGU PUBLICATIONS

JGR

Journal of Geophysical Research: Oceans

RESEARCH ARTICLE

10.1002/2014JC010055

Key Points:
- SPM concentration up to 300 g m^{-3} is retrieved using MERIS FR data
- Satellite SPM concentration is merged with oyster ecophysiological responses
- Offshore sites have a better potential for oyster-farming than intertidal zone

Correspondence to:
P. Gernez,
Pierre.Gernez@univ-nantes.fr

Citation:
Gernez, P., L. Barillé, A. Lerouxel, C. Mazeran, A. Lucas, and D. Doxaran (2014), Remote sensing of suspended particulate matter in turbid oyster-farming ecosystems, *J. Geophys. Res. Oceans*, *119*, 7277–7294, doi:10.1002/2014JC010055.

Received 14 APR 2014
Accepted 26 SEP 2014
Accepted article online 6 OCT 2014
Published online 29 OCT 2014

Remote sensing of suspended particulate matter in turbid oyster-farming ecosystems

Pierre Gernez[1], Laurent Barillé[1], Astrid Lerouxel[1], Constant Mazeran[2], Axel Lucas[3], and David Doxaran[3]

[1]Institut Universitaire Mer et Littoral (FR_C 3473), Mer Molécules Santé (EA 2160), Université de Nantes, Nantes, France, [2]ACRI-ST, Sophia-Antipolis, France, [3]Laboratoire d'Océanographie de Villefranche (UMR 7093), CNRS-UPMC, Villefranche sur Mer, France

Abstract High resolution satellite data of the Medium Resolution Imaging Spectrometer in full resolution mode (MERIS FR, pixel size is 300 m) were used to study the impact of suspended particulate matter (SPM) on oyster-farming sites in a macrotidal bay of the French Atlantic coast where SPM concentration can exceed 100 g m^{-3}. Because MERIS standard SPM concentration retrieval saturates at about 50 g m^{-3}, we developed an alternative method for turbid nearshore waters. The method consists in the combination of the Semi-Analytical Atmospheric and Bio-Optical (SAABIO) atmospheric correction with a regional bio-optical algorithm based on a linear relationship between SPM concentration and the reflectance band ratio at 865 and 560 nm. MERIS FR-derived SPM concentrations were validated from 10 up to 300 g m^{-3}, and then merged with oyster ecophysiological responses to provide a spatial picture of the impact of SPM concentration on oyster-farming sites. Our approach demonstrates the potential of high resolution satellite remote sensing for aquaculture management and shellfish-farming ecosystems studies.

1. Introduction

Accurate measurements of suspended particulate matter (SPM) concentration in turbid waters are a prerequisite for the environmental monitoring of nearshore areas, bathing waters, and navigational channels. As water quality parameter, turbidity, which depends on SPM concentration, is an operational indicator for the evaluation of the ecological status of coastal waters, as defined in policies of marine ecosystems integrated management, such as the European Water Framework Directive (2000/60/EC). Observing SPM concentration variations over a continuum of spatiotemporal scales, from a few meters to several kilometers, and from hours to years, improves our understanding of the structure and functioning of nearshore marine ecosystems. Turbidity reduces the penetration of solar irradiance within the water column and limits the photosynthetically available radiation for primary producers, including phytoplankton and microphytobenthos. In estuarine turbidity maximum zone, the concentration of dissolved oxygen can dramatically decrease as a result of negative balance between autotrophic and heterotrophic biological processes, thus negatively affecting marine organisms.

Variations in SPM concentration also influence the physiological responses of suspension-feeders such as oysters, mussels, and other filter-feeders [*Dubois et al*., 2009]. These organisms rely on suspended particles, trapped by their feeding structures, for their growth and reproduction [*Cranford et al*., 2011]. However, too high SPM concentrations negatively affect the ability of oysters to filter seawater, select and ingest particles [*Dutertre et al*., 2009a], in spite of phenotypic adaptation to cope with high turbidity conditions [*Dutertre et al*., 2009b]. Oyster clearance rate stops above an SPM concentration of about 200 g m^{-3} as a result of gill saturation, and particle selection efficiency, which allows oyster to preferentially select particulate organic matter before ingestion, decreases when SPM concentration exceeds 150 g m^{-3} [*Barillé et al*., 1997]. Satellite-derived maps of surface SPM concentration could be used in aquaculture spatial planning to identify farming sites with the most favorable SPM concentration for oyster growth. Due to the spatial coverage and timeframe of satellite observations, the value of satellite remote sensing for the management of marine resources has been emphasized in a number of recent publications [*Kapetsky and Aguilar-Manjarrez*, 2007, 2013]. For example, satellite-derived sea surface temperature and chlorophyll-*a* concentration can be used to predict spatiotemporal variability in mussel growth and to evaluate the suitability of coastal ecosystems

© 2014. American Geophysical Union. All Rights Reserved.

to shellfish aquaculture [*Thomas et al*., 2011]. However, the development of algorithms specifically adapted to turbid waters is an important requirement for aquaculture management and shellfish ecosystems studies because oyster-farming sites are often located within muddy intertidal environments characterized by important and highly variable SPM concentrations.

Due to ocean color satellite remote sensing, synoptic and spatially resolved maps of water reflectance can be used to monitor the changes of turbidity in coastal waters, which are caused by variations in the surface concentration of colored substances such as microalgae, colored dissolved organic matter, and suspended particulate matter. In turbid waters, SPM concentration remote sensing algorithms are usually based on empirical relationships established between SPM concentration and water reflectance at specific visible or near-infrared (NIR) wavelengths. The remote-sensing reflectance (R_{rs}), which is defined as the ratio between the water-leaving radiance to the downwelling irradiance just above sea surface, is at first-order proportional to the coefficient of backscattering and inversely proportional to the coefficient of absorption [*Morel and Prieur*, 1977]. As suspended particles absorb and scatter light in characteristic ways, R_{rs} is a suitable surrogate to determine SPM concentration using either in situ radiometers deployed under or above the air-water interface, or airborne, or satellite remote sensing.

In turbid waters where SPM concentration typically exceeds 50 g m^{-3}, the retrieval of R_{rs} from satellite remote sensing is mainly challenged by two issues associated with the existence of a significant water reflectance signal in the NIR (usually taken as the range 700–1000 nm). First, this affects atmospheric correction. In clear oceanic waters, the retrieval of aerosol reflectance is based upon the assumption that the NIR water-leaving radiance is equal to zero [*Gordon and Wang*, 1994]. This does not hold in turbid waters where NIR R_{rs} can significantly increase with SPM concentration [*Ruddick et al*., 2006]. Second, R_{rs} saturates in visible wavelengths when SPM concentration exceeds 50 g m^{-3} [*Shen et al*., 2010]. It is therefore recommended to shift to NIR wavelengths [*Ruddick et al*., 2006] where the correlation between R_{rs} and SPM allows the retrieval of SPM concentration over a larger range with a better accuracy [*Doxaran et al*., 2002]. In very turbid waters where SPM concentration exceeds 100 g m^{-3}, the R_{rs} signal in the short-wavelength infrared region (SWIR, 1000–3000 nm) can also be used to improve atmospheric correction [*Wang and Shi*, 2007], as well as the retrieval of SPM concentration [*Knaeps et al*., 2012] and inherent optical properties [*Shi and Wang*, 2014].

Another challenge of remote sensing in coastal waters relates to the difficulty of acquiring consistent data at relevant spatiotemporal scales. Nearshore areas are highly dynamic and the concentration, composition, and size distribution of marine particles typically undergo large variations [*Woźniak et al*., 2010], which are accompanied by correspondingly large variations in the intensity and shape of R_{rs} spectra. In macrotidal environments, resuspension of sediments occurs during the tidal cycle, inducing quarter-diurnal changes whose magnitude can exceed the seasonal range of surface SPM concentration variability [*Eleveld et al*., 2014]. A limited number of satellite images acquired at any time of the day regarding to the tidal cycle does not provide a representative picture of the range of SPM concentration in coastal areas influenced by tidal processes [*He et al*., 2013; *Ruddick et al*., 2014]. Tide-driven physical processes such as sediment transport and sea level variation also influence SPM variations at monthly time scales in coastal waters, and spring-neap SPM surface concentration variations are of the same order of magnitude than annual changes [*Rivier et al*., 2012; *Shi et al*., 2011, 2013; *Roberts et al*., 2014]. In such environments, measurement strategies designed to detect vertical and horizontal SPM variability including bottom sediment resuspension and vertical mixing within the water column are therefore needed to resolve the large range of SPM concentration that actually occurs in nearshore areas [*Schubel*, 1968]. Though satellite remote sensing cannot detect near-bed concentration, it can be used to study spatiotemporal variation of surface SPM concentration, and satellite-derived SPM maps are valuable tools to study the influence of SPM concentration in shallow waters influenced by tidal resuspension of bottom sediment and vertical mixing [*Fettweis and Nechad*, 2011].

We developed an SPM concentration algorithm for one of the most turbid oyster-farming area of the French Atlantic coast: Bourgneuf Bay, located south of the Loire estuary. Hyperspectral reflectance field data were used to develop a bio-optical relationship between SPM concentration and R_{rs} using a combination of wavelengths specific to the spectral bands of the Medium Resolution Imaging Spectrometer (MERIS). The algorithm was successfully validated at two oyster-farming sites, for a range of SPM concentration extending from 10 to 300 g m^{-3}. High resolution MERIS-derived maps of surface SPM concentration were then used to quantify the influence of turbidity on oyster growth in several oyster-farming sites of Bourgneuf Bay, and to suggest management operations.

© 2014. American Geophysical Union. All Rights Reserved.

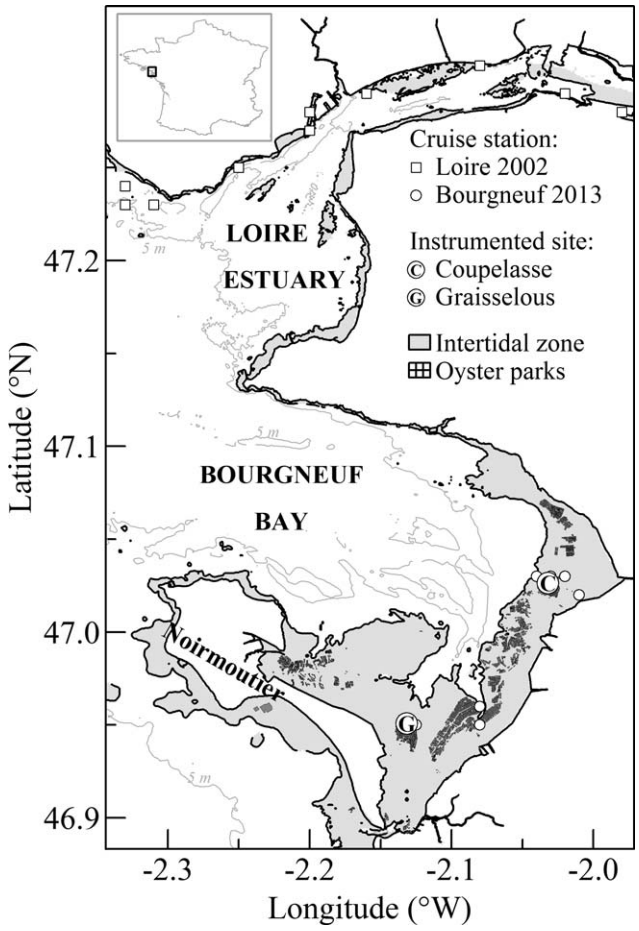

Figure 1. Map of the Loire estuary and Bourgneuf Bay on the French Atlantic coast, showing the intertidal zone (gray area), the location of oyster-farming sites (black grid), the 5 m depth contour line (gray line), the stations sampled during the bio-optical cruises in the Loire estuary in 2002 (white squares) and Bourgneuf Bay in 2013 (white circles), and the location of the two turbidity sensors deployed in 2005 and 2006 at the sites of La Coupelasse and Graisselous (circled letters C and G, respectively).

2. Data and Methods

2.1. Study Area

Located south of the Loire estuary, Bourgneuf Bay is a macrotidal bay with a tidal range varying from 2 to 6 m during neap and spring tides, respectively. The bay is connected to the ocean and to the Loire estuary in the north-west by an opening of 12 km, and closed in the south-west by the island of Noirmoutier, which is separated from mainland by a channel of 800 m of width (Figure 1). The surface area of the bay is 340 km^2, of which 100 km^2 of intertidal area are constituted mainly by mudflats. A rocky line divides the bay into two sectors of different hydro-sedimentary conditions. The northern sector is washed by highly turbid waters overlying intertidal mudflats, whereas the southern sector, less turbid, is mostly composed of intertidal sandy mudflats. At the site of La Coupelasse in the turbid northern sector, SPM annual mean concentration measured at about 0.7 m above bed sediments (corresponding to the height of oyster rack) is in the order of 150 g m^{-3}, whereas it is about 30 g m^{-3} at the site of Graisselous in the southern part of the bay [*Dutertre et al*., 2009a]. Particles composition also varies between the northern and southern sectors of the intertidal zone. Monthly mean concentration of particulate inorganic matter (PIM) accounts for 80–85% and 70–80% of the total SPM concentration at La Coupelasse and Graisselous, respectively [*Dutertre et al*., 2009a]. Grain size distribution of the bed sediments also differs between the two sectors: particles with mean diameter smaller than 44 μm account for $>$40% and $<$10% of the total weight of sediment at the sites of La Coupelasse and Graisselous, respectively [*Méléder et al*., 2005].

Intertidal mudflats of the Loire estuary and Bourgneuf Bay host microphytobenthos (MPB), that form biofilms dominated by assemblages of benthic diatoms at the surface of the sediment [*Méléder et al*., 2005; *Benyoucef et al*., 2013]. Resuspended MPB significantly contributes to the concentration of chlorophyll-*a* (Chl-*a*) measured in seawater samples, thus constituting an important trophic resource for oysters and other filter-feeder mollusks when phytoplankton abundance is limited by the environmental conditions [*Decottignies et al*., 2007]. In Bourgneuf Bay, oyster parks cover an area of 10 km^2 within the intertidal zone, and the bay yields an oyster production of about 8600 tons a year [*Agreste*, 2003], despite the negative influence of high SPM concentration on oyster growth and reproduction [*Dutertre et al*., 2009a; *Barillé et al*., 2011a].

2.2. In Situ Measurements

Two cruises were performed to acquire a data set of reflectance spectra and SPM concentration in turbid waters. The first cruise was conducted from 25 February to 1 March 2002 in the Loire estuary, as described in *Doxaran et al*. [2003]. The second cruise was conducted in Bourgneuf Bay from 8 to 12 April 2013 to study

© 2014. American Geophysical Union. All Rights Reserved.

how environmental parameters impact the functioning of oyster-farming ecosystems. During both cruises, water sampling and radiometric measurements were performed at nearshore stations located within the intertidal area (Figure 1) to acquire a wide range of SPM concentration data in conjunction with reflectance spectra. In Bourgneuf Bay, a traditional oyster-farming flat-bottomed barge was used to navigate throughout the shallow waters of the intertidal zone before low tide, and some stations were visited when the water depth was as low as 0.5 m. In these highly turbid waters, the bottom was never visible from above, even at the shallowest stations for which the Secchi depth was about 0.2 m.

The same method was used to measure reflectance spectra during the cruises in the Loire estuary and Bourgneuf Bay. Above-water radiometric measurements were conducted following NASA protocols [*Mueller et al*., 2002] to determine the spectral remote-sensing reflectance, $R_{rs}(\lambda)$, which was computed as

$$R_{rs}(\lambda)=[L_u^{0+}(\lambda)-\rho_{sky}L_{sky}^{0+}(\lambda)]/E_d^{0+}(\lambda) \tag{1}$$

where $L_u^{0+}(\lambda)$ is the upwelling radiance from the water and air-sea interface measured at a zenith angle of about 37°, $L_{sky}^{0+}(\lambda)$ is the sky radiance measured toward the region of sky that reflects into the seaviewing sensor, ρ_{sky} is the air-water interface reflection coefficient for radiance equal to the Fresnel reflection coefficient in the case of a flat sea surface, $E_d^{0+}(\lambda)$ is the above-water downwelling irradiance, and λ is the wavelength. The barge was maneuvered on station away from the sun to avoid shadowing effects. Radiance sensors were pointed at a solar azimuth angle between 90° and 135°. L_u^{0+}, L_{sky}^{0+}, and E_d^{0+} measurements were recorded simultaneously during about 5 min of apparently stable sky conditions using three TriOS-RAMSES hyperspectral spectroradiometers, two measuring the radiance signal and one measuring the downwelling irradiance.

A hyperspectral ASD spectroradiometer was also used in Bourgneuf Bay to acquire $R_{rs}(\lambda)$ data concomitantly with TriOS measurements. The same ASD sensor was used to measure L_u^{0+}, L_{sky}^{0+}, and the downwelling radiance at nadir, L_d^{0+}, during consecutive 2 min time series of data acquisition. L_u^{0+} and L_{sky}^{0+} were recorded by pointing the ASD sensor in the same directions as the TriOS sensors used to measure the upwelling and sky radiances, respectively. The ASD sensor was then pointed toward a white Spectralon plate to measure L_d^{0+}. E_d^{0+} was computed from L_d^{0+} multiplied by π and by the exact reflectance of the calibrated Spectralon plate, and R_{rs} was computed as in equation (1). A similar method to acquire $R_{rs}(\lambda)$ was used in the Loire estuary, where consecutive measurements of L_u^{0+}, L_{sky}^{0+}, and L_d^{0+} were performed using a single Spectron SE-590 spectroradiometer [*Doxaran et al*., 2003].

The ratio L_{sky}^{0+}/E_d^{0+} at 750 nm was used to discriminate clear from cloudy sky conditions following *Ruddick et al*. [2006], and only clear sky data were selected. Wave height was <0.5 m and wind speed was <5.0 m s^{-1} during both cruises. The ρ_{sky} coefficient was taken as 0.02 following *Austin* [1974]. A careful quality check was applied to the selected clear sky data which were then averaged over the time span of the measurements to obtain the mean value and standard deviation of R_{rs} at each station. The final output data of the TriOS measurements were the hyperspectral remote-sensing reflectance R_{rs} at a spectral resolution of 2.5 nm, from 305 to 950 nm. The final output data of the ASD measurements were the hyperspectral remote-sensing reflectance R_{rs} at a spectral resolution of 1 nm, from 350 to 2500 nm. The Fraunhofer absorption line around 761 nm corresponding to the dioxygen O_2-A band was removed from ASD reflectance spectra.

Seawater samples were collected just below the surface during optical measurements for subsequent laboratory determination of SPM concentration. Seawater samples were homogenized and stored in 1 l bottles until being analyzed in the laboratory in the afternoon. Measured volumes of seawater (between 25 and 100 mL depending of the turbidity of the sample) were filtered through preweighed GF/F glass-fiber filters. At the end of filtration, sample filters were rinsed with deionized water to remove sea salt. For the analysis of 2013 cruise samples, the turbidity, T (in Formazin Nephelometric Unit, FNU), of each water sample was determined in triplicate using a 2100Q portable turbidimeter (Hach Company, Loveland, CO, USA) in order to optimize the volume of filtered seawater, as in *Neukermans et al*. [2012]. SPM concentration, defined as the dry mass of particles per unit volume of seawater, was then determined using a standard gravimetric technique. The dry mass of particles collected on the filter was measured with a MT5 microbalance (Mettler-Toledo Intl. Inc.) with a resolution of 0.001 mg. The average particle mass retained on the filter was 4.73 mg while the mean filter dried mass was 26.0 mg. The measurement uncertainty was assumed to be the

© 2014. American Geophysical Union. All Rights Reserved.

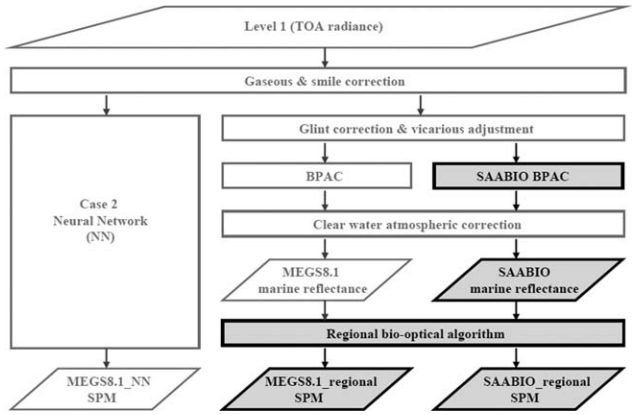

Figure 2. Scheme of MERIS data processing showing how the suspended particulate matter (SPM) concentration is computed from level 1 top-of-atmosphere (TOA) radiance data. MEGS8.1 processing steps are in white, changes specific to SAABIO or to the regional bio-optical algorithm are highlighted in gray. Three SPM concentrations were eventually computed, respectively, the MEGS8.1_NN, MEGS8.1_regional, and SAABIO_regional SPM concentrations.

standard deviation between triplicates (6%, on average), and a significant relationship between SPM concentration and *T* was obtained.

The seawater samples used to determine SPM concentration were collected concomitantly with hyperspectral R_{rs} measurements during both cruises. A regional bio-optical algorithm was developed from this data set to estimate SPM concentration from R_{rs} data in the Loire estuary and Bourgneuf Bay. The algorithm was based on a regional relationship between SPM concentration and $R_{rs}(865)/R_{rs}(560)$, a reflectance band ratio adapted to the spectral characteristics of the Medium Resolution Imaging Spectroradiometer (MERIS). The algorithm was applied to MERIS data (see next section), and validated using an independent data set of in situ SPM concentration. The validation data set consists in a 2 year turbidity time series at two oyster-farming sites in Bourgneuf Bay (La Coupelasse and Graisselous, Figure 1) where two oyster racks (i.e., oyster growing structure) were instrumented. Multiparameter water quality probes 6600 (YSI Inc., Yellow Springs, OH, USA) equipped with nephelometry sensor were deployed from 2005 to 2006 to perform autonomous turbidity measurement at an hourly frequency. SPM concentration was determined from turbidity using a linear relationship: SPM (g m^{-3}) $= 1.44 \times T + 12.92$, where *T* is the turbidity in nephelometric turbidity units (NTU). The relationship was obtained using a regression between turbidity and SPM concentration determined from concomitant seawater sampling, with a correlation coefficient (r^2) of 0.93, as described in *Dutertre et al.* [2009a]. The turbidity sensors were fixed at oyster racks' level at about 0.7 m above bottom. Sensor were inspected every month, and equipped with a flushing system to prevent biofouling. No drift was observed in the turbidity time series. At low tide, no data were acquired when the water depth was below the height of the oyster racks.

2.3. Processing of Satellite Data

MERIS level-2 data were downloaded from the Kalicôtier web portal (http://kalicotier.gis-cooc.org), which provides access to the complete archive of MERIS full resolution data (MERIS FR, pixel size is 300 m) on five coastal areas including the French Atlantic coast. Two processing chains are available and were considered in this study: the nominal European Space Agency's (ESA) third reprocessing [*MERIS Quality Working Group*, 2011], corresponding to processor version MEGS 8.1, and the alternative Semi-Analytical Atmospheric and Bio-Optical processing (SAABIO) provided as part of Kalicôtier by ACRI-ST [*Mazeran*, 2012]. The difference between MEGS 8.1 and SAABIO relates to the bright pixel atmospheric correction (BPAC) applied prior to the clear water atmospheric correction (Figure 2). Among the changes, the MEGS 8.1 BPAC uses three bands in the NIR [*Moore and Lavender*, 2011], whereas the SAABIO BPAC uses five bands in the visible and NIR (560, 620, 709, 775, and 865 nm) to avoid extrapolation of aerosol reflectance toward smaller wavelengths; this allows a better separation of the oceanic and atmospheric contributions from the top-of-atmosphere (TOA) radiance, and limits the risk of negative marine reflectance in the blue part of the spectrum. All other processing steps are strictly similar between MEGS 8.1 and SAABIO, in particular, the clear water atmospheric correction based on two NIR bands and providing marine reflectance in the visible spectral domain [*Antoine and Morel*, 1999] and its associated vicarious calibration factors (Figure 2).

SPM concentration was inversed from MEGS 8.1 or SAABIO marine reflectance using the regional bio-optical algorithm developed from the Loire estuary and Bourgneuf Bay data set, and two different SPM products were, respectively, computed, namely the MEGS8.1_regional and the SAABIO_regional products. The combination of SAABIO or MEGS 8.1 atmospheric correction with the regional bio-optical algorithm

© 2014. American Geophysical Union. All Rights Reserved.

constitutes an alternative to the neural network approach used in MEGS 8.1 for turbid waters [*Doerffer*, 2011], where SPM concentration is computed directly from TOA radiance data (Figure 2). For the sake of simplicity in the notation, the SPM concentration computed using the neural network inversion is hereafter named MEGS8.1_NN SPM concentration.

38 MERIS FR cloud free images over the study area were selected in 2005 and 2006 to observe surface SPM concentration in the intertidal zone of Bourgneuf Bay. Years 2005 and 2006 were chosen due to the existence of a large amount of in situ turbidity data acquired in the intertidal zone and available for validation. As SPM concentration variability in nearshore waters is characterized by significant fine-scale spatial variations [e.g., *Doxaran et al*., 2006], only the nearest MERIS FR pixel was extracted to compare SPM concentration derived from satellite radiometry with in situ turbidity measurements. The distance between the center of the extracted pixel and the location of the sampling point ranged from 20 to 223 m, with an average of 112 m and a standard deviation of 42 m. Given the importance of short time-scale variability associated with tidal dynamics, in situ hourly SPM concentration time series was interpolated to the exact time of MERIS overpass. Pixels flagged as cloud, land, ice haze, or high-glint were rejected.

A SPOT satellite image of Bourgneuf Bay acquired with the 20 m High Resolution Visible sensor (HRV2) during high tide on 13 December 2005 was selected to investigate MERIS subpixel spatial variability in the case of spatially heterogeneous SPM concentrations. SPOT level-2 data were computed using the Fast Line-of-Sight Atmospheric Analysis of Spectral Hypercubes (FLAASH) radiative transfer code [*Cooley et al*., 2002]. The FLAASH correction retrieves the sensor's gain and offset, as well as the geometric information from SPOT metadata. For each spectral band, the TOA upwelling radiance was corrected from atmospheric effects using the radiative transfer look-up tables of MODTRAN 4 (MODerate resolution atmospheric radiance and TRANsmittance model) [*Berk et al*., 1989]. The contribution of atmospheric constituents to the TOA radiance was estimated using a middle latitude winter atmospheric model and a maritime aerosol model parameterized with a visibility of 80 km. The final product derived from the FLAASH processing is the remote-sensing reflectance, R_{rs}, from which SPM concentration was computed using a specific relationship developed for SPOT-HRV2 in the Loire estuary [*Doxaran et al*., 2003]. SPOT-derived SPM concentration map was spatially averaged from its initial 20 m ground resolution to pixels of 300 or 1200 m, respectively, corresponding to the full or reduced resolution of MERIS images, in order to assess the degree of small-scale spatial variations within a MERIS pixel.

2.4. Coupling Satellite Data With Oyster Physiology

The MERIS FR imagery selected and validated in 2005 and 2006 were used to evaluate the potential impact of high SPM concentration on the main oyster-farming sites in Bourgneuf Bay. For each pixel of the satellite-derived SPM concentration maps, oyster clearance rate was computed following the model of *Barillé et al*. [1997] in which oyster clearance rate is negatively impacted by turbidity when SPM concentration exceeds two thresholds located at 60 and 200 g m^{-3} (Figure 3). A subset of 25 pixels was extracted over the main oyster-farming sites of Bourgneuf Bay, for which averaged oyster clearance rate and SPM concentration were analyzed to quantify the effect of SPM concentration on oyster growth. As all currently farmed oyster parks are located within the intertidal zone, an additional subtidal site was investigated outside the intertidal zone to assess the potential interest of offshore oyster-farming. The geographic coordinates of the offshore site correspond to the actual location of a mooring equipped with underwater cages that was recently tested for offshore oyster-farming (technical center for oyster-farming, P. Glize, personal communication, 2008).

3. Results

3.1. In Situ SPM Concentration and R_{rs} Variations

Annual variations of SPM concentration at the oyster-farming site of La Coupelasse are characterized by the absence of seasonal variability and by oscillations associated with springs-neaps tidal cycle (Figure 4a). Hourly averaged SPM concentration varies from $<$10 to $>$1500 g m^{-3} during a year whereas the concentration averaged over 1 tidal cycle spans a smaller range (10–500 g m^{-3}), thus highlighting the importance of tide-driven temporal variability at this nearshore site. In macrotidal environments, SPM variability is dominated by the resuspension, dilution, and concentration of mineral and organic sediments occurring

© 2014. American Geophysical Union. All Rights Reserved.

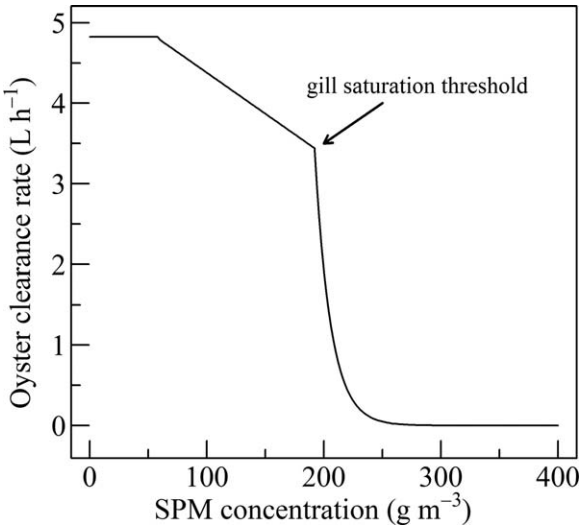

Figure 3. Modeled effect of suspended particulate matter (SPM) concentration on oyster clearance rate. The arrow at ~200 g m^{-3} shows the SPM concentration threshold at which oysters cannot filter anymore because of gill saturation (adapted from *Barillé et al*. [1997]).

throughout the bidiurnal tidal cycle [*Riaux-Gobin*, 1987]. SPM concentration varies in opposition with water height's tidal variations, reaching maximum at low tide and minimum at high tide (Figure 4b).

The large SPM variations are accompanied by important changes in the magnitude and spectral composition of remote-sensing reflectance, R_{rs} (Figure 5). Maximum R_{rs} is located between 575 and 590 nm, depending on SPM concentration, reaching 0.04 sr^{-1} at 590 nm when SPM concentration exceeds 250 g m^{-3}. The spectral width of the R_{rs} maximum plateau increases with SPM concentration, extending from 570 to 650 nm for the most turbid waters shown in Figure 4. This green-yellow plateau announces the saturation of R_{rs} in the visible domain [*Ruddick et al*., 2006]. Secondary reflectance maxima associated with the increase in SPM concentration occur at 810 and 1070 nm. Nonzero value of R_{rs} in the NIR is a known feature of turbid waters [*Doxaran et al*., 2002; *Wang and Shi*, 2007]. A secondary reflectance maximum in the SWIR at 1070 nm was previously observed in the turbid waters of the Scheldt River [*Knaeps et al*., 2012]. The hyperspectral R_{rs} spectra also display several features associated with the presence of pigment-bearing particles. The depression of R_{rs} around 675 nm is due to the absorption by chlorophyll-*a* (Figure 5). Another inflection in the slope of the reflectance spectra is also visible around 632 nm, attributable to the absorption by both chlorophyll-*a* and chlorophyll-*c*, a pigments association specific to diatoms [*Méléder et al*., 2005; *Barillé et al*., 2011b].

3.2. Development of a Regional Bio-Optical Algorithm for Turbid Waters

A total of 28 pairs of concomitant R_{rs} spectra and SPM concentration data have been gathered for the Loire estuary and Bourgneuf Bay. ASD measurements were not used in the development of the R_{rs} versus SPM bio-optical algorithm, though they favorably compare with TriOS data (Figure 5). Thanks to the acquisition of hyperspectral reflectance data, several combinations of R_{rs} at different wavelengths were tested to determine the most accurate relationship between SPM concentration and R_{rs}. The best empirical relationship for MERIS was obtained between SPM concentration and the 865–560 nm band ratio of remote-sensing reflectance, $R_{rs}(865)/R_{rs}(560)$ (Figure 6). The combination of the Loire estuary [*Doxaran et al*., 2003] and Bourgneuf Bay data sets yields a robust relationship ($r^2 = 0.98$) between SPM concentration and $R_{rs}(865)/R_{rs}(560)$ over a range of seston concentration spanning 1 order of magnitude from 25.4 to 527.3 g m^{-3}. The similarity of the two data sets suggests that the optical properties of suspended particles in the Loire estuary and Bourgneuf Bay are similar enough to develop a single regional bio-optical algorithm for the whole area (Figure 6). The existence of a single relationship all over the study area is noteworthy, given the hydrological heterogeneity of the stations sampled during the two cruises, which covered moderately to very turbid waters in the Loire estuary and intertidal oyster-farming sites in Bourgneuf Bay (Figure 1).

3.3. Evaluation and Application of the SPM Algorithm to MERIS FR Data

We remind here that three methods were evaluated to retrieve surface SPM concentration from MERIS data in the turbid waters of the Loire estuary and Bourgneuf Bay (Figure 2). MEGS8.1_NN SPM concentrations are severely underestimated in comparison with in situ measurements (Figure 7a), and the SPM concentration inversed using the neural network saturates when turbidity increases, rapidly reaching an upper limit around 50 g m^{-3}. The application of the regional bio-optical algorithm to the marine reflectance determined using either MEGS 8.1 or SAABIO atmospheric correction significantly improves SPM concentration

© 2014. American Geophysical Union. All Rights Reserved.

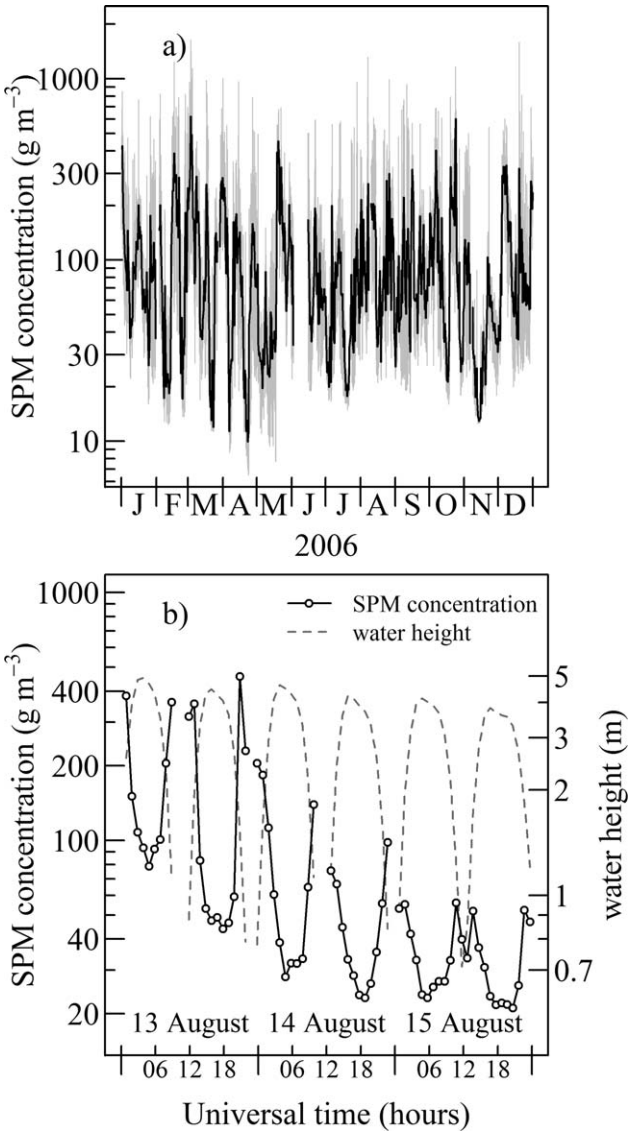

Figure 4. (a) Time series of in situ suspended particulate matter (SPM) concentration obtained from automated turbidity measurements at 0.7 m above bottom at La Coupelasse in 2006. Hourly averaged SPM concentration is in gray; average concentration over 1 tidal cycle is in black. (b) Example of a 3 day time series of SPM concentration from 13 to 15 August 2006. Within-day SPM concentration variation (in black) is associated with the tidal cycle of water height measured by a pressure sensor fixed at 0.7 m above bottom (dashed gray line). Note the absence of data at low tide when the turbidity and pressure sensors were above water.

determination (Figures 7b and 7c). The best algorithm is the combination of the SAABIO atmospheric correction with the regional bio-optical algorithm, and the comparison between in situ and SAABIO_regional SPM concentration is overall satisfactory over a wide range of seston concentration. No bias is observed between in situ and SAABIO_regional SPM concentration, and the regression line stays very close to the 1:1 line (Figure 7c).

A focus on few acquisitions spanning different turbidity regimes allows to better appraise the performance of the three methods (Figures 8 and 9). The difference of accuracy between the two regional methods is relatively low for moderately turbid waters with SPM concentration below 50 g m^{-3}, for which both MEGS8.1 and SAABIO atmospheric correction algorithms yield similar surface R_{rs} spectra (Figure 8a). The subsequent determinations of SPM concentration are roughly equivalent (Figure 8b). The accuracy of MEGS8.1 atmospheric correction degrades in turbid waters when SPM concentration reaches about 90 g m^{-3} (Figure 8c), and MEGS8.1_regional SPM concentration is underestimated by a factor of 2 (Figure 8d). The bright pixel atmospheric correction implemented within MEGS8.1 atmospheric correction fails when SPM concentration exceeds 200 g m^{-3}, yielding null $R_{rs}(\lambda)$ in the NIR (Figure 8e), which prevents the computation of SPM concentration from the $R_{rs}(865)/R_{rs}(560)$ band ratio (Figure 8f). The neural network inversion always returns an SPM concentration value, but it is systematically underestimated whatever the turbidity range (Figures 8b, 8d, and 8f). For the same MERIS FR pixels, the alternative SAABIO atmospheric correction yields consistent R_{rs} spectra (Figures 8a, 8c, and 8e), and the application of the regional bio-optical algorithm produces correct estimations over a range of SPM concentration spanning 1 order of magnitude from about 26 to 260 g m^{-3} (Figures 8b, 8d, and 8f).

The comparison of SPM concentration spatial distributions derived from the MEGS8.1_NN and SAABIO_regional methods further illustrates the underestimation of MERIS standard case 2 SPM algorithm, and its inadequacy to map SPM concentration in very turbid waters, on the contrary to the combination of SAABIO atmospheric correction and of the regional bio-optical algorithm, which detect spatial structures in the Loire

© 2014. American Geophysical Union. All Rights Reserved.

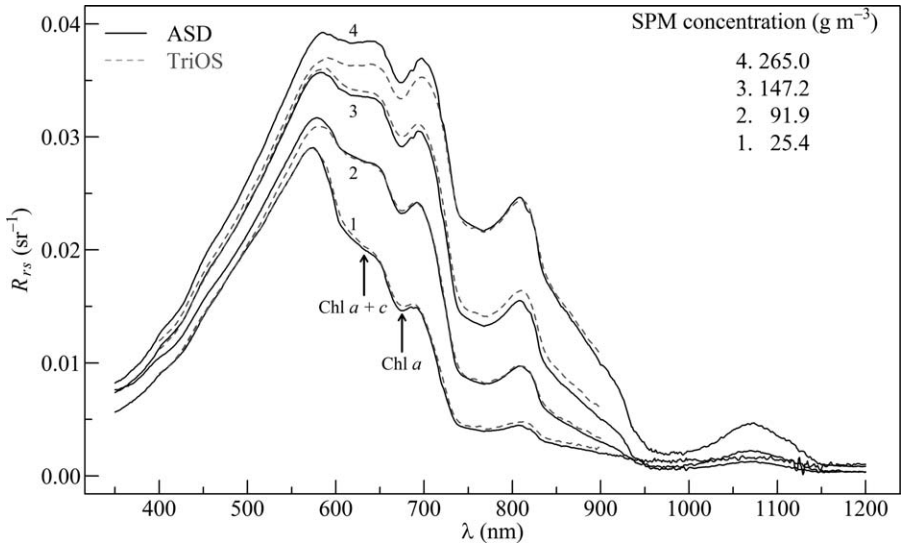

Figure 5. Examples of spectra of remote-sensing reflectance, $R_{rs}(\lambda)$, for moderately to very turbid waters in Bourgneuf Bay on 12 April 2013, acquired using an ASD or TriOS spectroradiometer. Arrows point to two significant absorption bands by chlorophyll-*a* and *c*.

estuary and Bourgneuf Bay (Figure 9). MEGS8.1_NN SPM concentration spans a limited range of values all over the study area, monotonously increasing shoreward from about 10 to 50 g m^{-3} (Figures 9a and 9c). MEGS8.1_NN SPM concentration does not exceed 50 g m^{-3}, even in the most turbid sectors of the Loire estuary and Bourgneuf Bay. The spatial distribution of MEGS8.1_NN SPM concentration is barely the same during neap and spring tide condition, whereas the resuspension of sediment particles by tidal currents is much lower during neap tide than during spring tide condition (Figures 8 and 9).

The same images processed using the combination of SAABIO atmospheric correction with the regional bio-optical algorithm display a wider range of SPM concentrations, up to 400 g m^{-3} (Figures 9b and 9d). During neap tide, SAABIO_regional SPM concentration exhibits the highest values at the fringe of the intertidal zone, notably in the turbid sectors of Les Moutiers, La Coupelasse, and Gril Nord (see Figure 10 for their location), consistently with the location of soft and noncohesive mudflats in Bourgneuf Bay. During spring tide, heterogeneous patches of turbid waters are detected over the intertidal zone, spreading high concentrations of seston offshore (Figures 9b and 9d). In the southern part of the bay, a turbid plume associated with tidal flow releases high loads of particles off the narrow channel between mainland and the island of Noirmoutier. The spatial distribution of surface SPM concentration in the Loire estuary is also more realistically displayed, showing fine-scale feature like the stretching of highly turbid water offshore along the southern side of the estuary (Figure 9). The turbid plume off the Loire estuary that is visible at the surface spreads to the west into the coastal ocean over a distance of about 10 km, even during neap tide condition (Figure 9). The improvement of SPM concentration retrieval within the

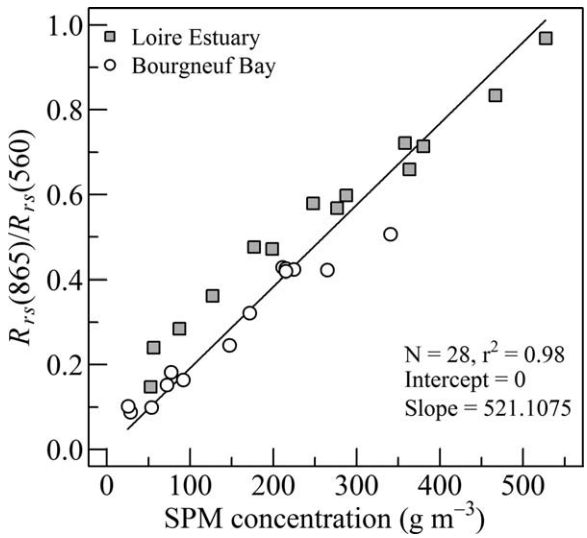

Figure 6. Suspended particulate matter (SPM) concentration versus band ratio of remote-sensing reflectance, $R_{rs}(865)/R_{rs}(560)$, in the Loire Estuary (gray squares) and Bourgneuf Bay (white circles). The black line shows the regression line.

© 2014. American Geophysical Union. All Rights Reserved.

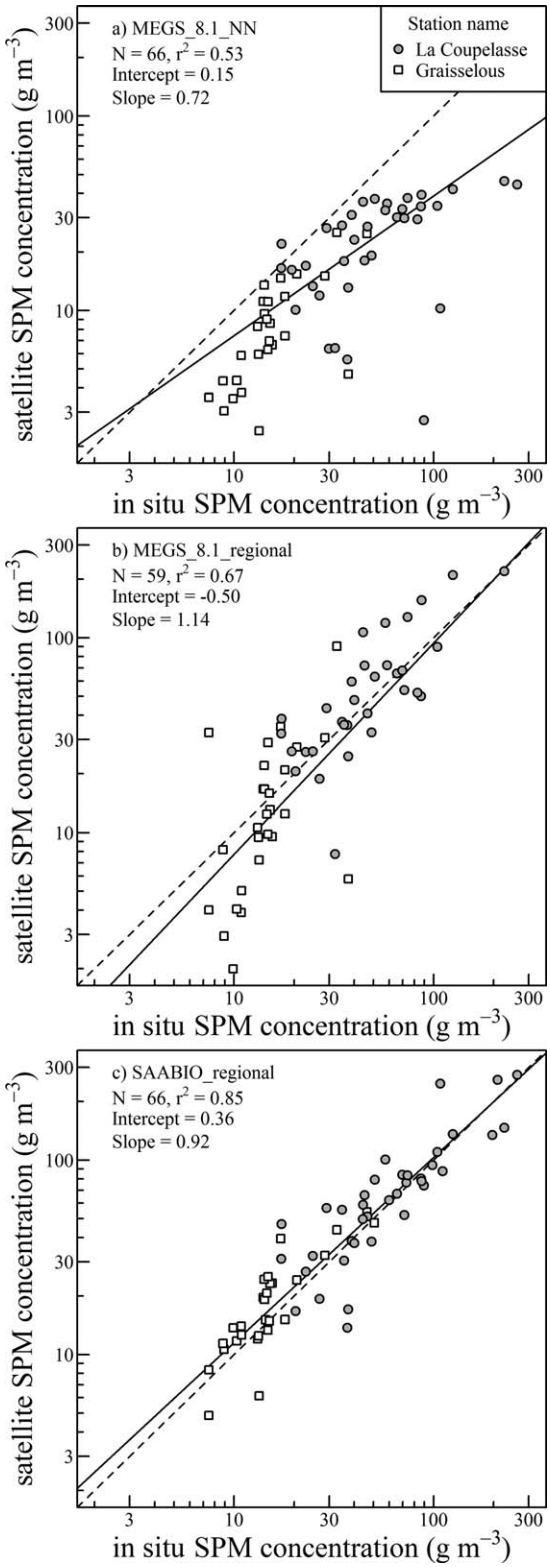

Figure 7. (a–c) For the intertidal stations of La Coupelasse and Graisselous, matchups of in situ suspended particulate matter (SPM) concentration obtained from nephelometry data versus MERIS FR-derived SPM concentration, using (a) MEGS8.1_NN, (b) MEGS8.1_regional, and (c) SAABIO_regional processing. The dashed line shows the 1:1 line, the continuous line shows the regression line.

intertidal zone using the SAABIO_regional method allows us to study the impact of high SPM concentration on oyster-farming sites, as presented in the next section.

3.4. Using High Resolution MERIS SPM Data for Oyster-Farming Spatial Planning

An example map of oyster clearance rate map derived from SAABIO_regional SPM concentration data is shown in Figure 10a. On this example, the spatial distribution of the modeled oyster clearance rate is highly contrasted. A constant maximum clearance rate of 4.8 L h^{-1} is reached wherever the SPM concentration is lower than 60 g m^{-3}, and the highest clearance rates are mainly distributed offshore. On the contrary, the modeled clearance rate decreases below 4 L h^{-1} in the intertidal zone, displaying large variations between and within intertidal oyster-farming sites. On this example, the maximal clearance rate is reached over three oyster-farming sites: Les Moutiers, Graisselous, and Paillard, whereas the minimum is located over the farming site of La Coupelasse, where the spatial variability is also maximal (Figure 10a).

In 2005 and 2006, farming site averaged oyster clearance rates ranged from $<$3.0 to 4.8 L h^{-1} (Figure 10b), with the offshore site, where surface SPM concentration never exceeded 20 g m^{-3}, having the highest value. The intertidal oyster-farming sites of Noirmoutier, Graisselous, and Paillard, all located in the southern part of the bay, ranked second in terms of clearance rate. The upper limit of SPM concentration at these sites was indeed consistently below the threshold value of 60 g m^{-3} at which oyster clearance rate generally starts to decrease [*Barillé et al.*, 1997]. Oyster clearance rate was altered at the oyster-farming sites of Ringeau and Gril Nord, which experienced moderate to high SPM concentrations. In the northern area of Bourgneuf Bay, the oyster-farming sites of Les Moutiers and La Coupelasse

© 2014. American Geophysical Union. All Rights Reserved.

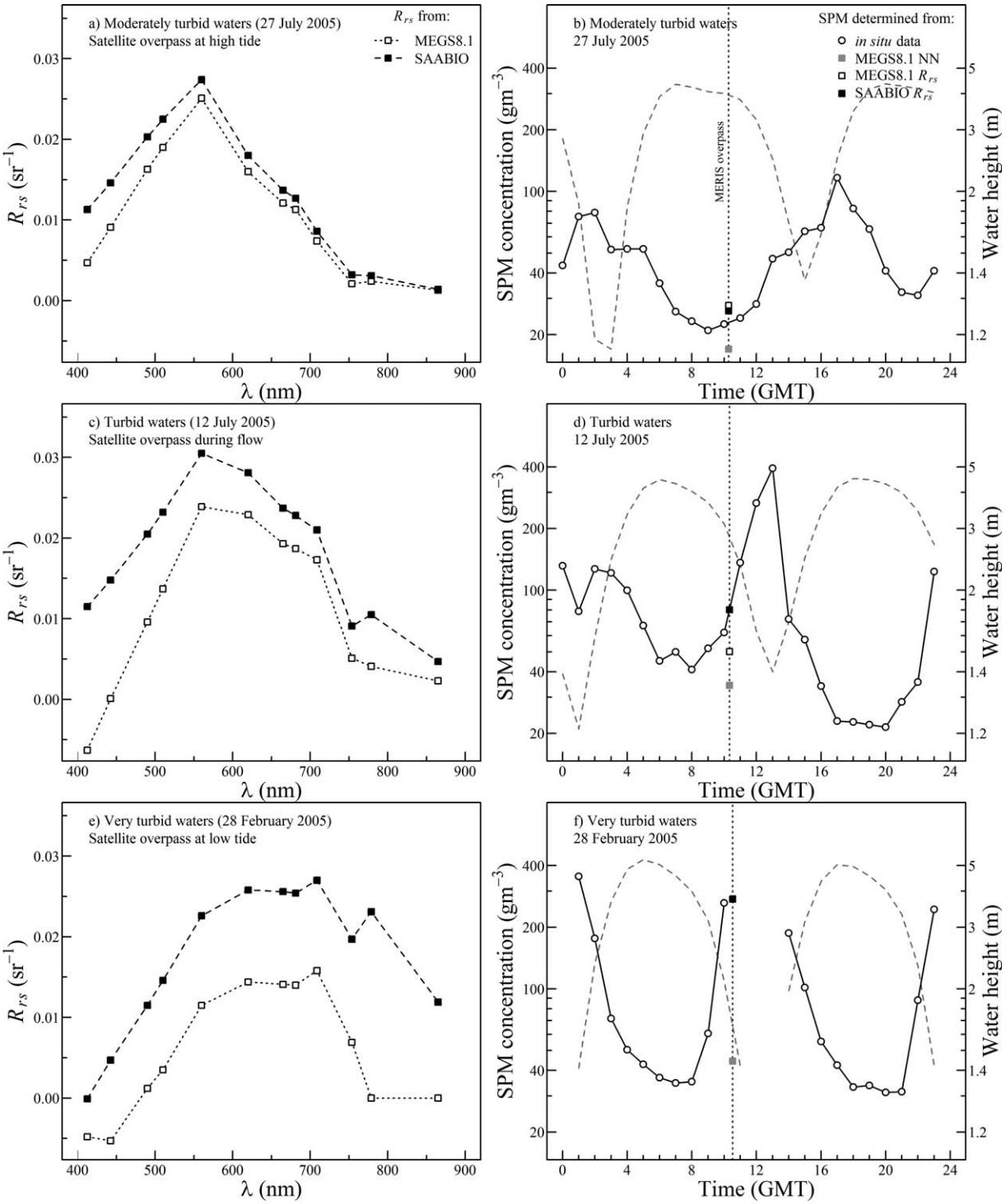

Figure 8. (a) For the moderately turbid waters of La Coupelasse at high tide on 28 July 2005, remote-sensing reflectance spectra, $R_{rs}(\lambda)$, extracted from a single MERIS FR pixel using either MEGS8.1 or SAABIO atmospheric correction. (b) For the same date and location, MERIS-derived suspended particulate matter (SPM) concentration obtained using MEGS8.1_NN (gray square), MEGS8.1_regional (white square), and SAABIO_regional (black square) processing at the time of satellite overpass are plotted on the daily time series of in situ SPM concentration (white circles) and water height measurements (dashed line). Same as in Figures 8a and 8b but (c, d) for turbid waters during tidal flow on 12 July 2005, and (e, f) for very turbid waters during low tide on 28 February 2005. Note the failure of the MEGS8.1 atmospheric correction (i.e., $R_{rs}(865)$ equals 0) and of the subsequent MEGS8.1_regional SPM concentration determination for very turbid waters (Figures 8e and 8f).

© 2014. American Geophysical Union. All Rights Reserved.

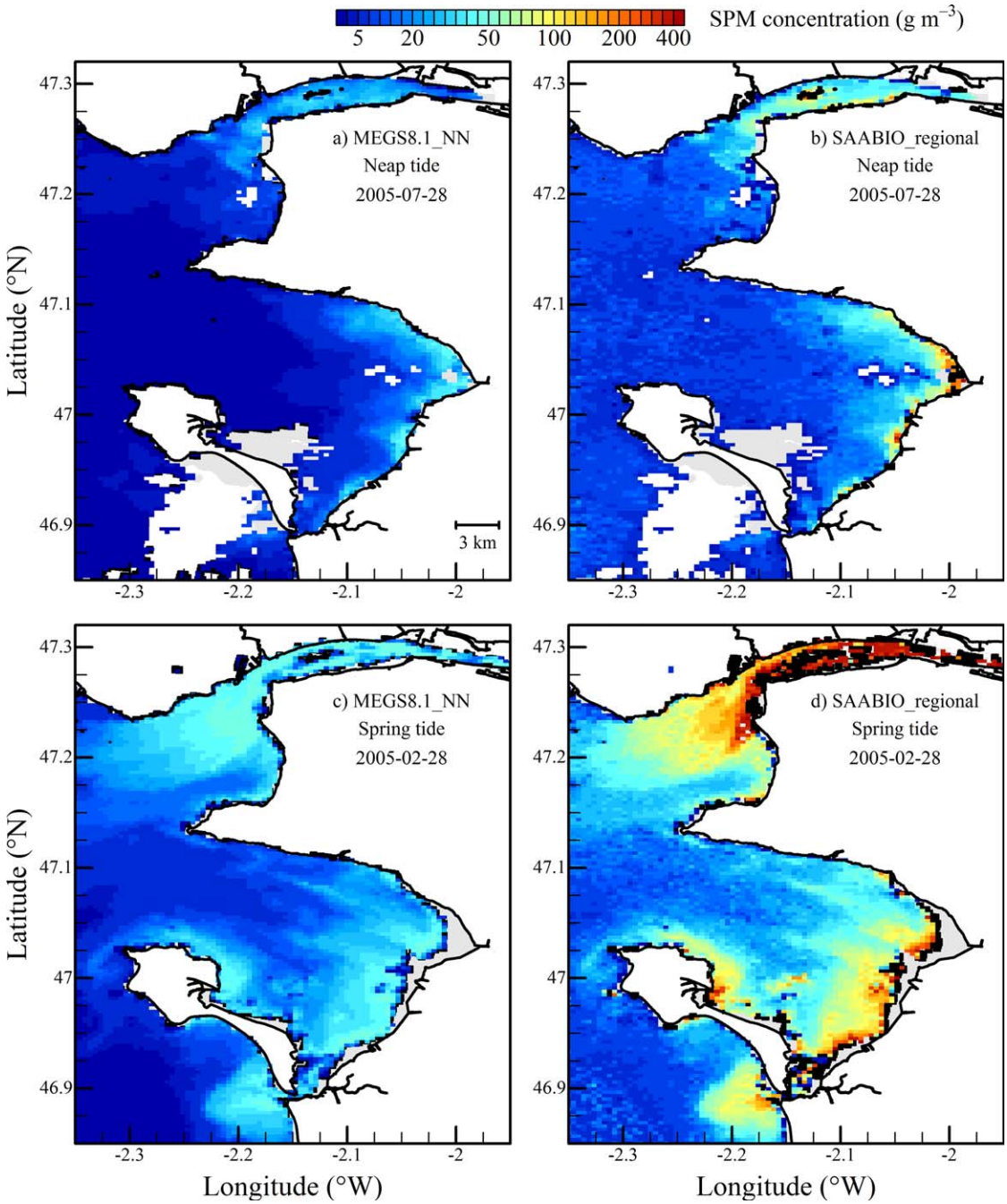

Figure 9. (a and b) During neap tide on 28 July 2005, map of suspended particulate matter (SPM) concentration computed using (a) either MEGS8.1 neural network, or (b) the combination of the SAABIO atmospheric correction with the regional bio-optical algorithm. The emerged part of the intertidal zone is in gray. White pixels correspond to clouds. (c, d) Same as in Figures 9a and 9b but during spring tide on 28 February 2005. In Figures 9b and 9d**,** black pixels correspond to points where $R_{rs}(865)$ and SPM concentration equal zero.

showed the lowest clearance rate, as low as 3 L h^{-1}. In these very turbid sectors SPM concentration often exceeded 200 g m^{-3}, a threshold value at which oyster gill saturation starts to occur [*Barillé et al.*, 1997].

4. Discussion

4.1. Remote Sensing of Nearshore Intertidal Areas

Intertidal and nearshore waters have rarely been observed from ocean color satellite sensors for several reasons. First, the spatial resolution of past and current ocean color sensors was generally not adapted to

© 2014. American Geophysical Union. All Rights Reserved.

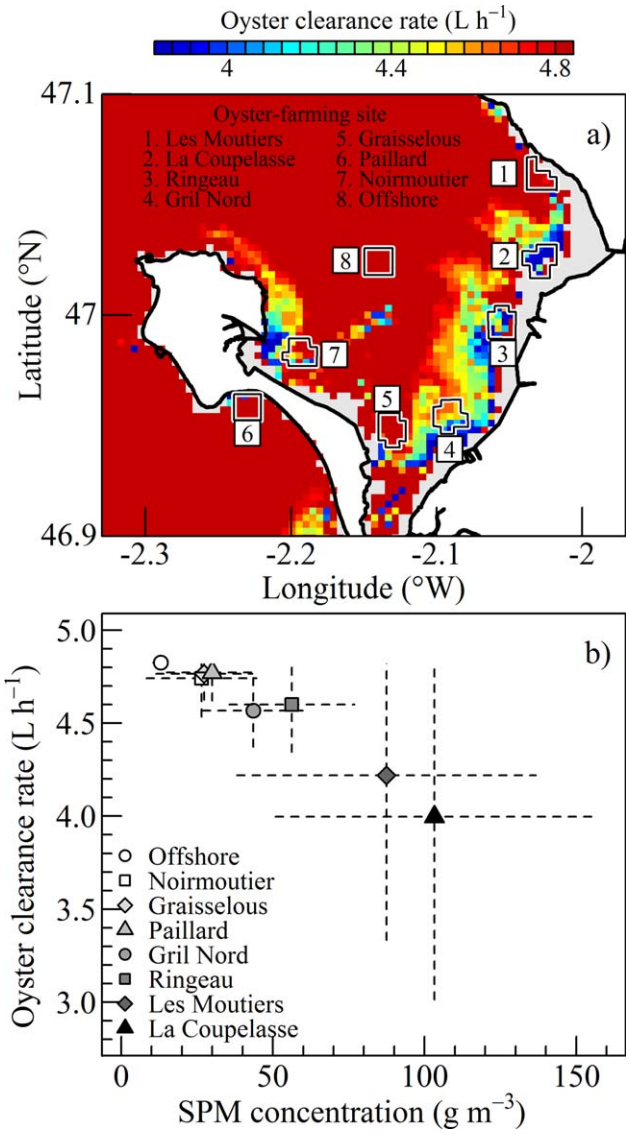

Figure 10. (a) Example of spatial distribution of modeled oyster clearance rate computed from MERIS FR SAABIO_regional SPM concentration on the 28 February 2005. The polygons show the location of the oyster-farming sites used in Figure 10b. (b) For the oyster-farming sites shown in Figure 10a, temporal average and standard deviation of the mean SPM concentration and oyster clearance rate computed using all MERIS FR data selected in 2005 and 2006.

coastal water research. The proximity to shore and the fineness of spatial details generally dismiss the use of sensors with spatial resolution coarser than about 300 m. Second, ocean color remote-sensing algorithms are generally challenged by atmospheric correction issues in turbid water with nonzero NIR reflectance. Third, bio-optical algorithms have been traditionally developed for lowly to moderately turbid waters, and they are not suited to retrieve SPM concentration above 50 g m^{-3}. Fourth, the limited number of cloud-free satellite images available during high-tide conditions dramatically reduces the number of matchups over intertidal areas.

Our study, however, demonstrates that the combination of the SAABIO alternative atmospheric correction with a regional bio-optical algorithm specifically designed for turbid waters makes it possible to retrieve SPM concentration up to 300 g m^{-3}, and to apply the results to ocean color satellite data. In order to assess the value of MERIS data to observe the spatial distribution of SPM surface concentration in oyster-farming areas, an example of SPOT-HRV2 SPM concentration map was spatially averaged at 300 and 1200 m ground resolutions, respectively, corresponding to MERIS full resolution (FR) and reduced resolution (RR) modes (Figure 11). The SPOT image was acquired near high tide and every oyster park within the intertidal zone was submerged by water. The spatial distribution of surface SPM concentration displays complex and heterogeneous patterns that are clearly visible due to the high spatial resolution (20 m) of SPOT-HRV2. The black rectangle in Figure 11a shows the turbid region-of-interest (ROI) selected to illustrate the changes in SPM spatial distribution observed at different scales. The comparison of the native resolution (20 m) and resampled data within the ROI clearly demonstrates the inability of the resolution of MERIS RR (1200 m) for nearshore oyster-farming studies, whereas the resolution of MERIS FR (300 m) is sufficient to catch the spatial details of surface SPM concentration over each oyster-farming site. The fine scale structure of the variation in SPM concentration along a 2 km coastward transect is clearly visible at 20 m resolution, still fairly visible at 300 m resolution, and completely blurred at 1200 m resolution (Figures 11 and 12). The degradation of spatial resolution from 20 to 300 m allows us to quantify MERIS FR subpixel variability. On this example, averaged MERIS FR subpixel spatial uncertainty is about 10%, locally reaching 30% in very dynamic

© 2014. American Geophysical Union. All Rights Reserved.

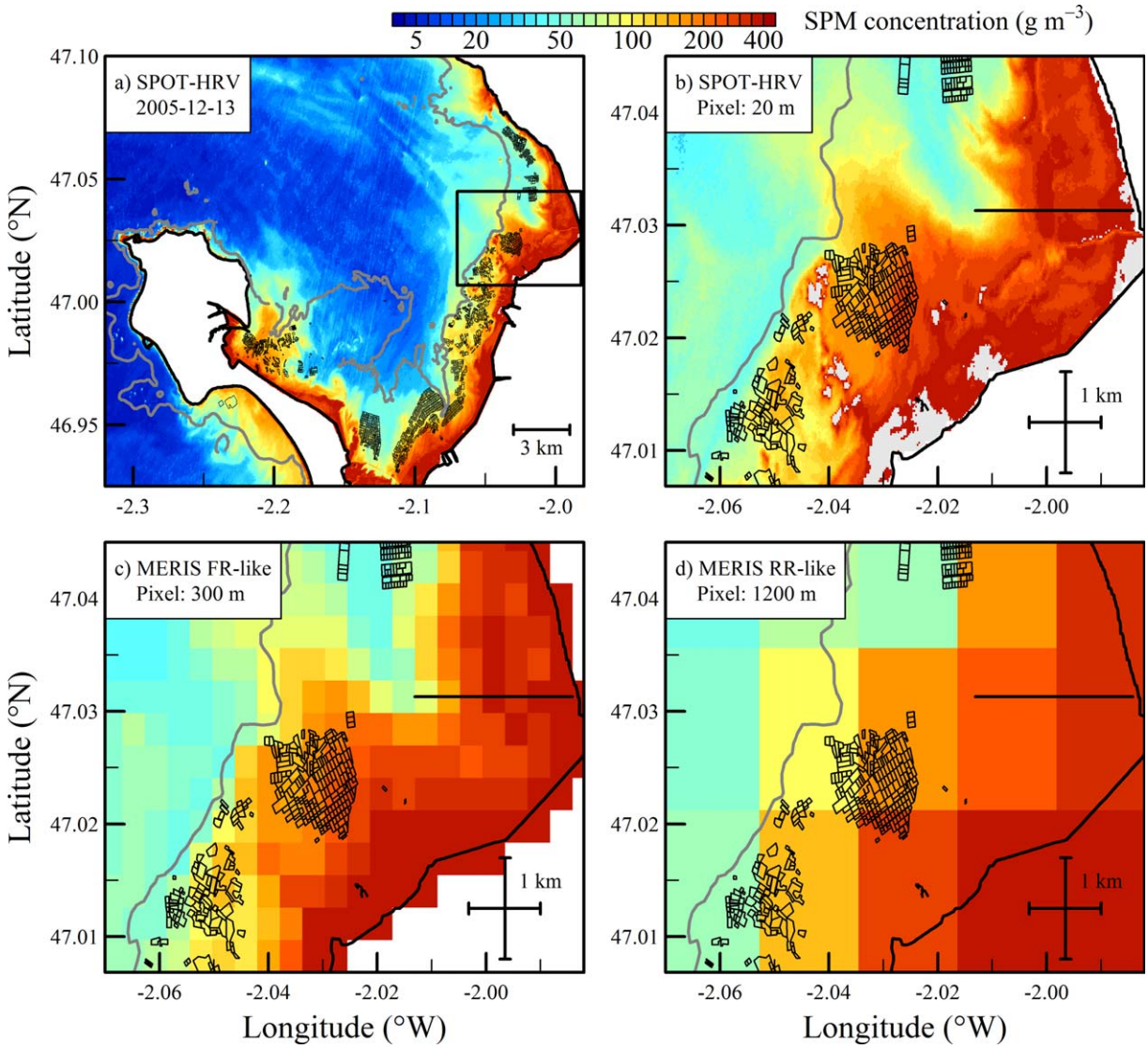

Figure 11. During high tide on 13 December 2005, SPOT-HRV2 map of suspended particulate matter (SPM) concentration showing (a) Bourgneuf Bay, and (b) a smaller region of interest near the oyster-farming parks of La Coupelasse. The location of oyster-farming growing structures is indicated by black polygons. One oyster park, the basic unit for oyster rearing, corresponds to a single polygon. The gray area shows the emerged part of the intertidal zone. The horizontal segment at about 47.03°N shows the transect used to compute SPM concentration variation in Figure 12. (c, d) Same as in Figure 11b, but the resolution has been degraded to 300 m and 1200 m to, respectively, simulate MERIS SPM concentration at full resolution (FR) and reduced resolution (RR).

areas where SPM concentration varies from 150 to 350 g m^{-3} within only 500 m (Figure 12b). The conclusion that 300 m is a relevant resolution for coastal zone research was recently drawn by *Vanhellemont and Ruddick* [2014] in a Landsat 8 study of SPM concentration spatial variations within an offshore wind farms array. Our analysis of the spatial scales of SPM concentration variation within an oyster-farming sector further demonstrates the potential of MERIS FR data for the environmental monitoring of nearshore areas.

Beyond HRV2 and MERIS, our approach could be extended to the next generation of ocean color satellite sensors such as the Multispectral Instrument (MSI) and the Ocean and Land Color Instrument (OLCI) that will be, respectively, launched in a near future onboard Sentinel 2 and 3 by ESA. Both MSI and OLCI spectral bands include the visible and NIR channels required for the SAABIO correction, and the bio-optical relationship between SPM concentration and $R_{rs}(865)/R_{rs}(560)$ could be easily adapted to the spectral bands of OLCI and MSI using the data set of hyperspectral R_{rs} spectra.

© 2014. American Geophysical Union. All Rights Reserved.

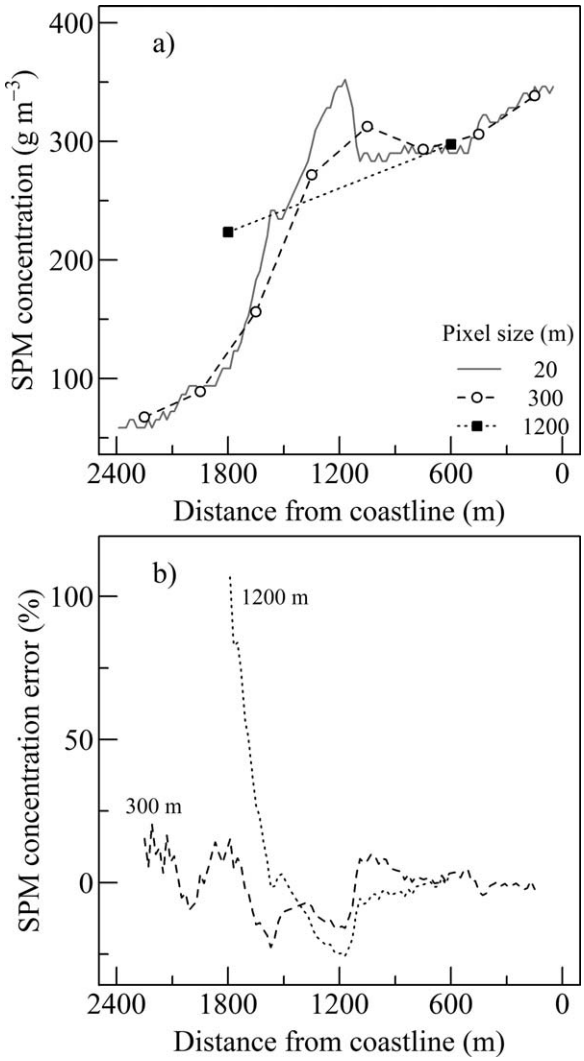

Figure 12. (a) Variation in suspended particulate matter (SPM) concentration along the shoreward transect shown in Figure 11b, observed at a resolution of 20, 300, or 1200 m. (b) SPM concentration error at a resolution of 300 or 1200 m along the same transect, compared to the native 20 m resolution.

The significant increase in reflectance at 1070 nm when SPM concentration exceeds 250 g m^{-3} (Figure 5) demonstrates the interest of using measurements of R_{rs} in the SWIR to retrieve SPM concentration in extremely turbid waters [*Knaeps et al*., 2012; *Shi and Wang*, 2014]. The portable ASD spectroradiometer, which covers a large visible and infrared spectral range from 350 to 2500 nm at a spectral resolution of 1 nm, is therefore particularly suited to develop bio-optical algorithm for very turbid waters. In a near future, the use of such spectroradiometer with extended spectral capacities will be useful to validate the OLCI reflectance band at 1020 nm. Hyperspectral data moreover offer the possibility to detect chlorophyll-*a* in turbid waters, even when particulate matter is dominated by mineral assemblages of mud and fine grain sediments. Chlorophyll-*a* and *c* absorption bands were indeed clearly visible on the R_{rs} spectra acquired in the intertidal waters of Bourgneuf Bay (Figure 5). The presence of these pigments in seawater, which was confirmed by High-Performance Liquid Chromatography (HPLC) analyses (data not shown), can be explained by the resuspension of benthic microalgae in the water column. Microphytobenthos form biofilms at the surface of intertidal mudflats, whose spatial distribution can be detected remotely, using either airborne [*Combe et al*., 2005], or satellite images acquired at high [*Méléder et al*., 2003] and moderate spatial resolution [*van der Wal et al*., 2010; *Brito et al*., 2013].

A limitation of satellite observation of intertidal waters is associated with the discrepancy between the time of satellite overpass and tidal cycle. Sun-synchronous polar orbiting sensors provide tidally biased observations in midlatitude tidal environment [*Eleveld et al*., 2014]. In Bourgneuf Bay, the time slot of satellite overpass (10:00–12:00) coincides with high-tide conditions during neap tides and with low-tide conditions during spring tides. MERIS observation of Bourgneuf Bay intertidal waters therefore mainly occurs during neap tides, thus leading to the under representation of SPM concentration variation, and to the subsequent under estimation of the actual impact of SPM on oyster physiological responses. In fact, for the selection of validated clear-sky and high-tide MERIS FR images, the tidal coefficient was generally low (mean: 61.7, standard deviation: 12.8, minimum: 23, maximum: 98). Interestingly, observations of surface SPM concentration from geostationary satellites [*Neukermans et al*., 2009; *Choi et al*., 2012; *He et al*., 2013; *Ruddick et al*., 2014; *Vanhellemont et al*., 2014] can overcome this limitation and provide data coincident with low-tide conditions whatever the tidal amplitude. In complement to ocean color satellite observations, the deployment

© 2014. American Geophysical Union. All Rights Reserved.

of automated in situ turbidity sensors in crucial areas could provide high-frequency data during all meteorological conditions [e.g., *Fettweis and Nechad*, 2011].

4.2. Using Ocean Color Satellite Data for Oyster-Farming Studies

Ideally, the modeling of other oyster ecophysiological functions requires SPM concentration, sea surface temperature (SST), and chlorophyll-*a* concentration (Chl-*a*). Maps of satellite-derived SST, Chl-*a*, and SPM concentration could therefore be used to map oyster growth in oyster-farming areas. Several ecophysiological models including the Dynamical Energy Budgets (DEB) and the Scope for Growth (SFG) have been successfully used to simulate oyster growth in several oyster-farming areas along the French coast [*Alunno-Bruscia et al*., 2011] including Bourgneuf Bay [*Barillé et al*., 2011a]. The modeling approach is not restricted to oyster-farming, and could be extended to other shellfish species, such as cockles [*Troost et al*., 2010], mussels [*Rosland et al*., 2009], or scallops [*Bacher et al*., 2003]. Surprisingly, the combination of shellfish ecophysiological modeling with ocean-color satellite remote sensing has been rarely investigated, despite the wide range of expected applications in aquaculture [*Grant et al*., 2007, 2009]. *Thomas et al*. [2011] recently spatialized DEB simulations of mussel growth at 1 km spatial resolution using NOAA18-derived SST and SeaWiFS-derived Chl-*a* concentration in the moderately turbid and large embayment of Mont Saint Michel Bay within the French Atlantic coast.

To our knowledge, our remote-sensing analysis is the first study to address oyster-farming issues using high resolution ocean color satellite data. Assessing the impact of SPM concentration on oyster-farming in such turbid waters was only possible due to the successful development of a regional bio-optical algorithm, which was specifically designed to retrieve SPM concentration up to 300 g m^{-3} in the intertidal waters where oyster parks are located. Such study would have not been possible using the standard MERIS case 2 SPM concentration product, which saturates at about 50 g m^{-3}. The satellite-derived spatial distribution of oyster clearance rate in Bourgneuf Bay confirms that oyster-farming sites located in the northern sector of the bay are more impacted by too high SPM concentrations than the sites located in the southern area, an observation previously made from in situ oyster growth studies [*Haure and Baud*, 1995; *Barillé-Boyer et al*., 1997]. These in situ oyster growth experiments were however limited to two geographic locations, and the satellite analysis provides a spatially resolved picture of the response of oyster to high SPM concentration. Our analysis demonstrates that oysters reared offshore would be much less altered by high SPM concentration than oysters farmed within the intertidal zone, thus confirming the potential of offshore oyster-farming in alternative to traditional farming in turbid intertidal environments.

5. Conclusions

While the influence of SPM concentration on the physiological responses of suspension-feeders has mostly been assessed through laboratory experiments, it has rarely been studied at the scale of shellfish-farming ecosystems. We demonstrated that high resolution satellite data can be merged with oyster ecophysiological responses to provide a consistent spatial picture of the impact of SPM concentration between oyster-farming sites. Specifically, our major findings are:

1. A regional algorithm was developed and successfully applied to MERIS FR data to retrieve surface SPM concentration up to 300 g m^{-3} in the Loire estuary and Bourgneuf Bay.
2. MERIS-derived SPM concentration maps were merged with oyster ecophysiological responses to study the impact of high SPM concentration on oyster-farming sites all over Bourgneuf Bay.
3. Offshore sites, which are currently not used for oyster-farming, have a better potential for oyster growth than the traditionally farmed intertidal oyster-farming sites.

The approach presented here is only a first attempt to use satellite observations for the spatial planning of marine resources, and it opens new perspectives for aquaculture management and shellfish-farming ecosystems studies. As satellites have the ability to observe the world ocean at a global scale as well as to zoom in specific coastal areas, the combination of high resolution satellite observations with bivalves ecophysiological model could make it possible to spatially explore the response of cultivated suspension-feeders to environmental conditions in every region of the planet, at a spatial scale compatible with the size of shellfish-farming sites.

© 2014. American Geophysical Union. All Rights Reserved.

Acknowledgments
We thank Philippe Rosa and Anthony Le Bris for their help during the field measurements in Bourgneuf Bay. The field cruise in the Loire estuary was led by Jean-Marie Froidefond and funded by the "Cellule de Mesure et de Bilans, Loire Estuaire," which is now the "GIP Loire Estuaire." The bio-optical cruise in Bourgneuf Bay was funded by the French Research National Agency in the frame of the GIGASSAT project (ANR-12-AGRO-0001-05 and ANR-12-AGRO-0001-08). MERIS level-2 products and statistics were processed by ACRI-ST and distributed on the GIS COOC data portal in the frame of the Kalicôtier project, funded by CNES, using ESA ENVISAT MERIS FR data. The SAABIO atmospheric correction was developed at ACRI-ST by Marcel Babin and Constant Mazeran with CNES cofundings. We thank the CNES for the ISIS Program regarding the use of SPOT satellite data. MERIS FR data for this paper are available on the GIS COOC Kalicôtier web portal: http://kalicotier.gis-cooc.org/. In situ data are available upon request to Pierre Gernez (pierre.gernez@univ-nantes.fr). We thank David Bowers and one anonymous reviewer for helpful comments on the paper.

References

Agreste (2003), *Recensement de la conchyliculture en 2002*, Minist. de l'Agric., de l'Alimentation, de la Pêche et des Affaires Rurales, Paris.

Alunno-Bruscia, M., Y. Bourlès, D. Maurer, S. Robert, J. Mazurié, A. Gangnery, P. Goulletquer, and S. Pouvreau (2011), A single bio-energetics growth and reproduction model for the oyster *Crassostrea gigas* in six Atlantic ecosystems, *J. Sea Res.*, *66*, 340–348.

Antoine, D., and A. Morel (1999), A multiple scattering algorithm for atmospheric correction of remotely-sensed ocean colour (MERIS instrument): Principle and implementation for atmospheres carrying various aerosols including absorbing ones, *Int. J. Remote Sens.*, *20*, 1875–1916.

Austin, R. W. (1974), Inherent spectral radiance signatures of the ocean surface, in *Ocean Color Analysis*, 195 pp., Scripps Inst. of Oceanogr., La Jolla, Calif.

Bacher, C., J. Grant, A. J. Hawkins, J. Fang, M. Zhu, and M. Besnard (2003), Modelling the effect of food depletion on scallop growth in Sungo Bay (China), *Aquat. Living Resour.*, *16*, 10–24.

Barillé, L., M. Héral, and A.-L. Barillé-Boyer (1997), Modélisation de l'écophysiologie de l'huître *Crassostrea gigas* dans un environnement estuarien, *Aquat. Living Resour.*, *10*, 31–48, IFREMER, Nantes, France.

Barillé, L., A. Lerouxel, M. Dutertre, J. Haure, A.-L. Barillé, S. Pouvreau, and M. Alunno-Bruscia (2011a), Growth of the Pacific oyster (*Crassostrea gigas*) in a high-turbidity environment: Comparison of model simulations based on scope for growth and dynamic energy budgets, *J. Sea Res.*, *66*, 392–402.

Barillé, L., J.-L. Mouget, V. Méléder, P. Rosa, and B. Jesus (2011b), Spectral response of benthic diatoms with different sediment backgrounds, *Remote Sens. Environ.*, *115*, 1034–1042.

Barillé-Boyer, A.-L., J. Haure, and J.-P. Baud (1997), L'ostréiculture en baie de Bourgneuf, Relation entre la croissance des huîtres Crassostrea gigas et le milieu naturel: Synthèse de 1986 à 1995, *IFREMER Rep. DRV/RA/RST/97-16*. [Available at http://archimer.ifremer.fr/doc/00000/1633/.]

Benyoucef, I., E. Blandin, A. Lerouxel, B. Jesus, P. Rosa, V. Méléder, P. Launeau, and L. Barillé (2013), Microphytobenthos interannual variations in a north-European estuary (Loire estuary, France) detected by visible-infrared multispectral remote sensing, *Estuarine Coastal Shelf Sci.*, *136*, 43–52.

Berk, A., L. S. Bernstein, and D. C. Robertson (1989), MODTRAN: A Moderate Resolution Model for LOWTRAN7, *Final Rep. GLTR-0122*, Air Force Geophysics Laboratory (AFGL), Hanscom Air Force Base, Burlington, Md.

Brito, A. C., I. Benyoucef, B. Jesus, V. Brotas, P. Gernez, C. R. Mendes, P. Launeau, M. P. Dias, and L. Barillé (2013), Seasonality of microphytobenthos revealed by remote-sensing in a South European estuary, *Cont. Shelf Res.*, *66*, 83–91.

Choi, J.-K., Y. J. Park, J. H. Ahn, H.-S. Lim, J. Eom, and J.-H. Ryu (2012), GOCI, the world's first geostationary ocean color observation satellite, for the monitoring of temporal variability in coastal water turbidity, *J. Geophys. Res.*, *117*, C09004, doi:10.1029/2012JC008046.

Combe, J. P., P. Launeau, V. Carrère, D. Despan, V. Méléder, L. Barillé, and C. Sotin (2005), Mapping microphytobenthos biomass by non-linear inversion of visible-infrared hyperspectral images, *Remote Sens. Environ.*, *98*, 371–387.

Cooley, T., et al. (2002), FLAASH, a MODTRAN4-based atmospheric correction algorithm, its application and validation, in *Proceedings of the International Geoscience and Remote Sensing Symposium*, vol. 3, Toronto, Canada, pp. 1414–1418, IEEE (Institute of Electrical and Electronics Engineers, Inc., Piscataway, N. J.

Cranford, P. J., J. Ward, and S. E. Shumway (2011), Bivalve filter-feeding: Variability and limits of the aquaculture filter, in *Shellfish Aquaculture and the Environment*, edited by S. E. Shumway, pp. 81–133, John Wiley, Chichester, U. K.

Decottignies, P., P. G. Beninger, Y. Rincé, and P. Riera (2007), Trophic interactions between two introduced suspension-feeders, *Crepidula fornicata* and Crassostrea gigas, are influenced by seasonal effects and qualitative selection capacity, *J. Exp. Mar. Biol. Ecol.*, *342*, 231–241.

Doerffer, R. (2011), Alternative atmospheric correction procedure for case 2 water remote sensing using MERIS, MERIS ATBD 2.25, Issue 1. [Available at http://earth.esa.int/envisat/instruments/meris/atbd.]

Doxaran, D., J.-M. Froidefond, S. J. Lavender, and P. Castaing (2002), Spectral signature of highly turbid waters: Application with SPOT data to quantify suspended particulate matter concentrations, *Remote Sens. Environ.*, *81*, 149–161.

Doxaran, D., J.-M. Froidefond, and P. Castaing (2003), Remote sensing reflectance of turbid sediment-dominated waters: Reduction of sediment type variations and changing illumination conditions effects using reflectance ratios, *Appl. Opt.*, *42*, 2623–2634.

Doxaran, D., P. Castaing, and S. J. Lavender (2006), Monitoring the maximum turbidity zone and detecting fine-scale turbidity features in the Gironde estuary using high spatial resolution satellite sensor (SPOT HRV, Landsat ETM+) data, *Int. J. Remote Sens.*, *27*, 2303–2321.

Dubois, S., L. Barillé, and B. Cognie (2009), Feeding response of the polychaete *Sabellaria alveolata* (Sabellariidae) to changes in seston concentration, *J. Exp. Mar. Biol. Ecol.*, *376*, 94–101.

Dutertre, M., P. G. Beninger, L. Barillé, M. Papin, P. Rosa, A.-L. Barillé, and J. Haure (2009a), Temperature and seston quantity and quality effects on field reproduction of farmed oysters, *Crassostrea gigas*, in Bourgneuf Bay, France, *Aquat. Living Resour.*, *22*, 319–329.

Dutertre, M., L. Barillé, P. Beninger, P. Rosa, and Y. Gruet (2009b), Variations in the pallial organ sizes of the invasive oyster, *Crassostrea gigas*, along an extreme turbidity gradient, *Estuarine Coastal Shelf Sci.*, *85*, 431–436.

Eleveld, M. A., D. van der Wal, and T. van Kessel (2014), Estuarine suspended particulate matter concentrations from sun-synchronous satellite remote sensing: Tidal and meteorological effects and biases, *Remote Sens. Environ.*, *143*, 204–215.

Fettweis, M. P., and B. Nechad (2011), Evaluation of in situ and remote sensing sampling methods for SPM concentrations, Belgian continental shelf (southern North Sea), *Ocean Dyn.*, *61*, 157–171.

Gordon, H. R., and M. Wang (1994), Retrieval of water-leaving radiance and aerosol optical thickness over the oceans with SeaWiFS: A preliminary algorithm, *Appl. Opt.*, *33*, 443–452.

Grant, J., G. Bugden, E. Horne, M. C. Archambault, and M. Carreau (2007), Remote sensing of particle depletion by coastal suspension-feeders, *Can. J. Fish. Aquat. Sci.*, *64*, 387–390.

Grant, J., C. Bacher, J. G. Ferreira, S. Groom, J. Morales, C. Rodriguez-Benito, S. Saitoh, S. Sathyendranath, and V. Stuart (2009), Remote sensing applications in marine aquaculture, in *Remote Sensing in Fisheries and Aquaculture, Rep. of the Int. Ocean-Colour Coord. Group 8*, edited by M.-H. Forget, V. Stuart, and T. Platt, pp. 77–88, Canadian Space Agency (CSA), Dartmouth, Nova Scotia, Canada.

Haure, J., and J.-P. Baud (1995), Approche de la capacité trophique dans le bassin ostréicole (Baie de Bourgneuf), *IFREMER Rep. RIDRV-95-16/RA-BOUIN*, IFREMER, Nantes, France. [Available at http://archimer.ifremer.fr/doc/00000/6441/.]

He, X., Y. Bai, D. Pan, N. Huang, X. Dong, J. Chen, C.-T. A. Chen, and Q. Cui (2013), Using geostationary satellite ocean color data to map the diurnal dynamics of suspended particulate matter in coastal waters, *Remote Sens. Environ.*, *133*, 225–239.

Kapetsky, J. M., and J. Aguilar-Manjarrez (2007), Geographic information systems, remote sensing and mapping for the development and management of marine aquaculture, *FAO Fish. Tech. Pap.* 458, Food and Agriculture Organization of the united nations (FAO), Rome.

 © 2014. American Geophysical Union. All Rights Reserved.

Kapetsky, J. M., and J. Aguilar-Manjarrez (2013), From estimating global potential for aquaculture to selecting farm sites: Perspectives on spatial approaches and trends, in *Site Selection and Carrying Capacities for Inland and Coastal Aquaculture*, edited by L. G. Ross et al., pp. 129–146, Food Agric. Organ., Rome.

Knaeps, E., A. I. Dogliotti, D. Raymaekers, K. Ruddick, and S. Sterckx (2012), *In situ* evidence of non-zero reflectance in the OLCI 1020 nm band for a turbid estuary, *Remote Sens. Environ.*, *120*, 133–144.

Mazeran, C. (2012), Kalicôtier, SAABIO processing, *Tech. Note Ref. A1037-TN-010-ACR*. [Available at http://kalicotier.gis-cooc.org/kalicotier_static/A1037-NT-010-ACR_v1.0.pdf.]

Méléder, V., P. Launeau, L. Barillé, and Y. Rincé (2003), Cartographie des peuplements du microphytobenthos par télédétection spatiale visible-infrarouge dans un écosystème conchylicole, *C. R. Biol.*, *326*, 377–389.

Méléder, V., L. Barillé, Y. Rincé, M. Morançais, P. Rosa, and P. Gaudin (2005), Spatio-temporal changes in microphytobenthos structure analysed by pigment composition in a macrotidal flat (Bourgneuf Bay, France), *Mar. Ecol. Prog. Ser.*, *297*, 83–99.

MERIS Quality Working Group (2011), MERIS 3rd data reprocessing, software and ADF updates, *Ref. A879.NT.008.ACRI-ST*. [Available at http://earth.eo.esa.int/pcs/envisat/meris/documentation/meris_3rd_reproc/.]

Moore, G., and S. J. Lavender (2011), Case 2 (sediment) bright water atmospheric correction, *MERIS ATBD 2.6 Issue 5.0* [Available at https://earth.esa.int/instruments/meris/atbd/atbd_2.6.pdf.]

Morel, A., and L. Prieur (1977), Analysis of variations in ocean color, *Limnol. Oceanogr.*, *22*, 709–722.

Mueller, J. L., et al. (2002), Above-water radiance and remote-sensing reflectance measurements and analysis protocols, in *Ocean Optics Protocols for Satellite Ocean Color Sensor Validation, Revision 3*, edited by G. S. Fargion and J. L. Mueller, pp. 171–182, NASA Goddard Space Flight Cent., Greenbelt, Md.

Neukermans, G., K. Ruddick, E. Bernard, D. Ramon, B. Nechad, and P. Y. Deschamps (2009), Mapping total suspended matter from geostationary satellites: A feasibility study with SEVIRI in the Southern North Sea, *Opt. Express*, *17*, 14,029–14,052.

Neukermans, G., K. Ruddick, H. Loisel, and P. Roose (2012), Optimization and quality control of suspended particulate matter concentration measurement using turbidity measurements, *Limnol. Oceanogr. Methods*, *10*, 1011–1023.

Riaux-Gobin, C. (1987), Phytoplancton, tripton et microphytobenthos: Échanges au cours de la marée, dans un estuaire du Nord-Finistère (Phytoplankton, tripton, and microphytobenthos: Exchanges during the tidal cycle in a North-Finistere (Brittany) estuary), *Cah. Biol. Mar.*, *28*, 159–184.

Rivier, A., F. Gohin, P. Bryère, C. Petus, N. Guillou, and G. Chapalain (2012), Observed *vs*. predicted variability in non-algal suspended particulate matter concentration in the English Channel in relation to tides and waves, *Geo Mar. Lett.*, *32*, 139–151.

Roberts, E. M., D. G. Bowers, and A. J. Davies (2014), Springs-neaps cycles in daily total seabed light: Daylength-induced changes, *J. Mar. Syst.*, *132*, 116–129.

Rosland, R., Ø. Strand, M. Alunno-Bruscia, C. Bacher, and T. Strohmeier (2009), Applying Dynamic Energy Budget (DEB) theory to simulate growth and bio-energetics of blue mussels under low seston conditions, *J. Sea Res.*, *62*, 49–61.

Ruddick, K., G. Neukermans, Q. Vanhellemont, and D. Jolivet (2014), Challenges and opportunities for geostationary ocean colour remote sensing of regional seas: A review of recent results, *Remote Sens. Environ.*, *146*, 63–76.

Ruddick, K. G., V. De Cauwer, Y. J. Park, and G. Moore (2006), Seaborne measurements of near infrared water-leaving reflectance: The similarity spectrum for turbid waters, *Limnol. Oceanogr. Methods*, *51*, 1167–1179.

Schubel, J. R. (1968), Turbidity maximum of the northern Chesapeake Bay, *Science*, *161*, 1013–1015.

Shen, F., S. Salama, Y. Zhou, J. Li, Z. Su, and D. Kuang (2010), Remote-sensing reflectance characteristics of highly turbid estuarine waters? A comparative experiment of the Yangtze River and the Yellow River, *Int. J. Remote Sens.*, *31*, 2639–2654.

Shi, W., and M. Wang (2014), Ocean reflectance spectra at the red, near-infrared, and shortwave infrared from highly turbid waters: A study in the Bohai Sea, Yellow Sea, and East China Sea, *Limnol. Oceanogr. Methods*, *59*, 427–444.

Shi, W., M. Wang, and L. Jiang (2011), Spring-neap tidal effects on satellite ocean color observations in the Bohai Sea, Yellow Sea, and East China Sea, *J. Geophys. Res.*, *116*, C12032, doi:10.1029/2011JC007234.

Shi, W., M. Wang, and L. Jiang (2013), Tidal effects on ecosystem variability in the Chesapeake Bay from MODIS-Aqua, *Remote Sens. Environ.*, *138*, 65–76.

Thomas, Y., J. Mazurié, M. Alunno-Bruscia, C. Bacher, J.-F. Bouget, F. Gohin, S. Pouvreau, and C. Struski (2011), Modelling spatio-temporal variability of *Mytilus edulis* (L.) growth by forcing a dynamic energy budget model with satellite-derived environmental data, *J. Sea Res.*, *66*, 308–317.

Troost, T. A., J. W. M. Wijsman, S. Saraiva, and V. Freitas (2010), Modelling shellfish growth with dynamic energy budget models: An application for cockles and mussels in the Oosterschelde (southwest Netherlands), *Philos. Trans. R. Soc. B*, *365*, 3567–3577.

van der Wal, D., A. Wielemaker-van den Dool, and P. M. Herman (2010), Spatial synchrony in intertidal benthic algal biomass in temperate coastal and estuarine ecosystems, *Ecosystems*, *13*, 338–351.

Vanhellemont, Q., and K. Ruddick (2014), Turbid wakes associated with offshore wind turbines observed with Landsat 8, *Remote Sens. Environ.*, *145*, 105–115.

Vanhellemont, Q., G. Neukermans, and K. Ruddick (2014), Synergy between polar-orbiting and geostationary sensors: Remote sensing of the ocean at high spatial and high temporal resolution, *Remote Sens. Environ.*, *146*, 49–62.

Wang, M., and W. Shi (2007), The NIR–SWIR combined atmospheric correction approach for MODIS ocean color data processing, *Opt. Express*, *15*, 15,722–15,733.

Woźniak, S. B., D. Stramski, M. Stramska, R. A. Reynolds, V. M. Wright, E. Y. Miksic, M. Cichocka, and A. M. Cieplak (2010), Optical variability of seawater in relation to particle concentration, composition, and size distribution in the nearshore marine environment at Imperial Beach, California, *J. Geophys. Res.*, *115*, C08027, doi:10.1029/2009JC005554.

 © 2014. American Geophysical Union. All Rights Reserved.